Chapter 3
Metamaterial-Based Vibration Mitigation for Enhanced Reliability of an Automotive Inverter: A Numerical Study

Sara Tincani, Claus Claeys, Elke Deckers, Nimish Pandiya, and Christian Dindorf

Abstract This paper investigates the deployment of locally resonant metamaterials on an electric drivetrain power electronics unit to attenuate structural vibrations on critical sub-components on the Printed Circuit Board (PCB) through simulation-driven investigations. The PCB comprises of a copper foil layer laminated with insulating materials, onto which various electronically functional components (such as transistors, diodes, and resistors) are soldered. Operational vehicle loads lead to critical vibration levels on the PCB plate at resonances, which are composed of both local (only PCB plate) and global (across the whole assembly) modes. Such loads are causes of sensor breakage on the PCB in terms of vibration reliability and lead to functional failures.

Traditionally, metamaterial solutions are mostly designed as periodic structures, applied locally and uniformly to the component requiring vibration reduction. However, such a direct, traditional application of repeated unit cells on the PCB is impractical due to operational and design constraints. This necessitates an alternative approach where the vibration mitigation system is applied to a different sub-component in the assembly in a non-uniform matter to shield the PCBs from critical zones. Hence, the feasibility of such an adaptation of metamaterial design to the spider-frame (a die-casted part that secures the PCB to the assembly) is examined.

The required mass increase and strategic placement of unit cells (UCs) are studied. Hereto different realizable resonators are compared. Furthermore, the results obtained with a realizable locally resonant metamaterial (LRM) concept are compared against idealized tuned vibration absorber (TVA). Vibration reduction is shown to be achieved via addition of metamaterials to the spider by means of a comparative frequency response function (FRF) analysis against the original design concept.

Keywords Locally Resonant Metamaterials, Tuned Vibration Absorbers, Reliability, Printed Circuit Board, E-mobility

Introduction

During their service life, electronic components in electric vehicles are subjected to vibrational loads that require in-depth analysis and testing to ensure their reliability during their operational lifetime [1]. The principal reason for damage occurring is the difference in bending characteristics between the Printed Circuit Board (PCB) and the electronic components soldered to it [2], [3]. Different studies have been conducted both experimentally and through simulation to consider the reliability

Sara Tincani · Nimish Pandiya · Christian Dindorf
Robert Bosch GmbH, Center of Competence-Vibration, Robert-Bosch-Straße 2, 71701 Schwieberdingen, Germany
e-mail: sara.tincani@de.bosch.com; Nimish.Pandiya@de.bosch.com; christian.dindorf@de.bosch.com

Claus Claeys
KU Leuven, Department of Mechanical Engineering, Celestijnenlaan 300 - box 2420, Heverlee, Belgium
e-mail: claus.claeys@kuleuven.be

Claus Claeys · Elke Deckers
Flanders Make@KU Leuven, Belgium
e-mail: claus.claeys@kuleuven.be; elke.deckers@kuleuven.be

Sara Tincani · Elke Deckers
KU Leuven Campus Diepenbeek, Department of Mechanical Engineering, Wetenschapspark 27, 3590 Diepenbeek, Belgium
e-mail: sara.tincani@de.bosch.com; elke.deckers@kuleuven.be

Matthew Allen et al. (eds.), *Special Topics in Structural Dynamics & Experimental Techniques, Vol. 5*, Conference Proceedings of the Society for Experimental Mechanics Series, https://doi.org/10.13052/97887-438-0150-4_3

of these components leading to proposed solutions for robust bonding between sensors and the PCB, surface treatment, or stiffening of the supporting structure [4], [5]. These solutions typically involve chemical treatments or time-consuming design modifications implemented for the PCB's sensors connections.

The work presented in this paper focuses on the possibility of exploiting novel, lightweight vibration control solutions to reduce the critical vibrational load in certain frequency ranges, which would be critical for the described components. In this regard, locally resonant metamaterials (LRMs) have been extensively studied in the past decade and have attracted (majorly) academic treatment and attention due to their ability to combine lightweight design and excellent NVH (noise, vibration, and harshness) behavior in targeted frequency ranges. These frequency ranges of interest, also called stop bands, are zones where no free wave propagation is allowed via targeted modification of the object's structural dynamics [6].

This is achieved mainly through two different approaches:

- Bragg scattering interference [7]: at frequencies where the Bragg condition is satisfied, stop bands may be created by ensuring low transmission of waves through the presence of zones with destructive interference between reflected and transmitted waves. This is the mechanism on which the creation of stop bands in photonic and phononic crystals is based.
- Resonance based approaches: due to Fano-type interference between wave propagating in the host structure and re-radiated waves by resonant additions to the host [8] [9], stop bands with vibrational attenuation are created. This type of material structures are typically referred to as LRMs [6].

While photonic crystals are significantly dependent on the length scale of periodicity, this is not the case with LRMs, which, due to their dependency on resonant phenomena, can enable stop bands by additions on a sub-wavelength scale. [9]. For these reasons, LRMs prove to be a promising solution for vibration reduction, especially in low-frequency, practical applications.

Various real-world scenarios of LRM implementations in the automotive sector for low-frequency airborne and structure-borne noise, and vibration reduction are present in literature [11] and are reviewed for this work. The vehicle cabin interior vibration attenuation by use of mass-spring systems is investigated through simulations by Wu et al. [12]. Effective reduction of structure-borne noise in the vehicle cabin and low frequency noise mitigation in tires are reported in the work of Sangiuliano et al. [13], [14] through numerical and experimental studies. Jung et al. [15] and Riess et al. [16] report reduction of air-borne noise by exploiting the implementation of LRM solutions on car body panels and doors respectively.

LRMs have been proved to be effective lightweight performance solution capable of improving NVH behavior over targeted frequency ranges, ensuring, if necessary, a compact design. Moreover, thanks to the possibility of using various production technologies such as additive manufacturing or injection molding [17], [18] and different materials, they can represent a valuable solution to vibrational problems for multiple industrial applications. Extending the concept described in the literature, a motivated investigation of LRMs on electronic components for reduction of vibrational load is warranted especially to ensure improved component reliability. In particular, the present simulation-based study investigates the potential of an LRM solution to reduce the vibrational load experienced on the PCB of an electric drive power electronics unit, especially when it is subject to a global mode of the structure. The most critical modes of the PCB are analyzed and various LRM solutions that can be implemented on the component, are proposed and compared via a numerical study.

The paper is outlined as follows: in Section 2 the problem is presented, and the component is described, both in terms of the typical NVH behavior of the structure and the definition of the frequency range of interest. The constraints to be respected in the design of the solution are highlighted. In Section 3 a single tuned vibration absorber (TVA), modeled as a mass-spring system, and a LRM concept, realized using idealized mass-spring systems, are compared. The results indicate the LRM solution as the best alternative. Section 4 presents two different LRM designs. Their dispersion curves are presented, and their performance is compared to an idealized TVA-case in order to determine the best performing design type. Thereafter, the optimal solution, that guarantees an improvement to the vibrational response of the component, is selected. In Section 5 the LRM solution chosen in the previous section is applied to the component, and the simulation on the entire structure discussed. Finally, in Section 6, the findings of the simulations are summarized along with an outlook for future work.

Problem Definition

The PCB as a part of the Power Electronic Unit (PEU) assembly (also referred to as inverter), exhibits both global modes (modes involving the entire structure) and local modes (where only the PCB and the sensors placed on it are affected) in the frequency range of interest. For the present treatment, a global mode of the structure is considered. For confidentiality reasons only the PCB mounted on the die-casted spider plate is shown (regarding these images, they represent a generic geometry, not specific to the product). For simulations, however, the complete PEU assembly is evaluated.

Fig. 1 shows the assembly composed of the spider frame and PCB, and the frame only. In particular, the latter is the component of interest for the implementation of the LRM solution since a direct application on the PCB is not practical. This is due to the complexity of the component itself and the infeasibility of making direct modifications to it. This work therefore considers the addition of resonators on the spider, tuned to act on a global out-of-plane mode of the (PCB + spider) sub-assembly where high displacements are seen to occur. Considering the complexity of the frame, which has various ribs and holes and is not characterized by a continuous surface, it is investigated how an efficient LRM solution would reduce the system response. To determine the feasibility of the solution, a (theoretical) LRM concept, modeled as a grid of spring-mass systems (TVAs), is compared with the implementation of a single TVA, and the different effects are compared (in the work presented, when referring to TVAs, it refers to idealized mass-spring systems).

Furthermore, two different design goals are set for the implementation of the LRM solution:

1. The total amount of mass added due to the resonators should not exceed around 15% of the assembly mass. The resonators should be producible by an efficient manufacturing process.
2. Considering the presence of the PCB screwed on the frame, the dimensions of the resonator are constrained by the space available between the two components.

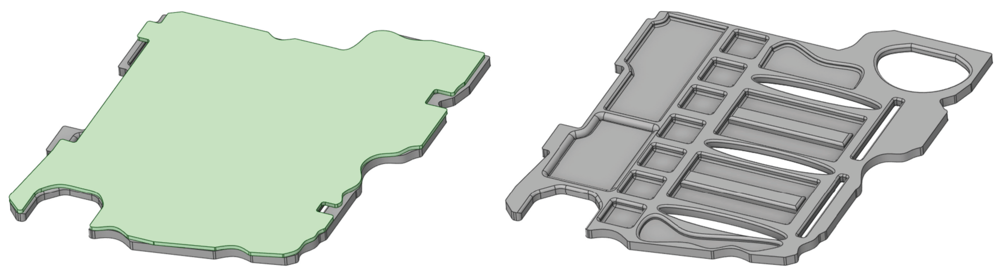

Fig. 1 Left: Sub-assembly: Frame and PCB. Right: Frame.

LRM Solution And Single Tuned Vibration Absorber: Comparison

In the initial phase of the study, both the LRM and the single-TVA were modeled using mass-spring systems. Ansys is used for all simulations described hereafter. The simplicity of the lumped-mass resonators permits a quick evaluation of the effectiveness of the proposed solutions and provide comparisons of their effectiveness on the structure. The lumped masses are modeled using MASS21 elements, while the springs are modeled using COMBIN14 elements. The ends of the spring elements are connected to the point mass and to the component in the desired and defined positions through a remote point. The total mass addition corresponds to 15% of the mass of the assembly. In all three considered configurations, the stiffness of the springs is adjusted so that the resonance frequency of each TVA is equal to the frequency at which the out-of-plane mode of the structure occurs: to obtain a stopband on the frequency range of interest it is necessary that the resonators introduce a localized resonant behavior in the host structure [3]. The exact frequency value is excluded in the present discussion due to confidentiality reasons and is replaced by $\mathrm{f_{res}}$.

An important consideration regards the scale at which the resonant elements operate in relation to the wavelength of vibrations they are intended to mitigate: for a structure, to be an effective LRM solution, and hence exhibit stop band behavior, the size of the spacing between the resonant elements should be smaller than the wavelength of the waves they are going to affect [6].

The three cases are distinguished as follows:

1. In the first case, all the added mass is concentrated in a single TVA, which is placed in the central zone of the frame (also the zone subject to the maximum deformation at $\mathrm{f_{res}}$). The single TVA does not directly relate to the theoretical LRM concept, as it focuses on localized mass addition rather than a periodic arrangement of elements.
2. In the second case, the added mass is equally divided among 25 TVAs. This case represents the maximum number of TVAs that can be realistically added, given constraints imposed by the geometry of the component, and have been also positioned where resonators could be placed in a real case scenario. The wavelength of interest is influenced by factors such as the material properties of the frame, the boundary conditions, and the operational environment, making a precise, universal definition of subwavelength challenging for this kind of application. However, given the physical

dimensions of the frame and the spacing between the TVAs, this concept is considered within the subwavelength regime for the range of frequencies considered.

3. In the third case, the added mass is equally divided among 50 TVAs. Placement of 50 TVAs is physically unrealistic as the added TVAs would cover the entire spider plate. Even so, this case is considered to evaluate the behavior and effect of a classic LRM concept. On average the spacing between the TVAs in this case can be similar as in case 2.

The three cases considered are shown in Fig. 2.

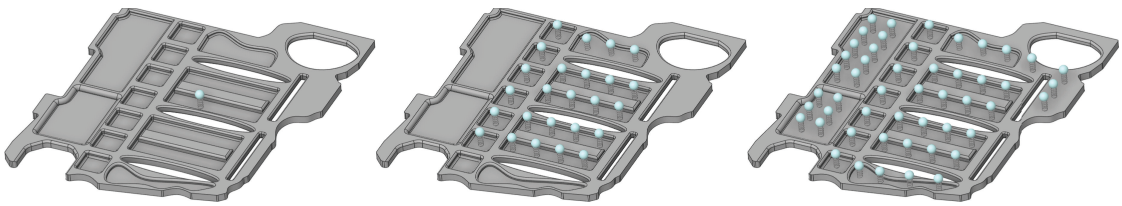

Fig. 2 Single TVA configuration. Center: 25 TVAs configuration. Right: 50 TVAs configuration.

For all three described configurations, a constant force with a magnitude of 1 N is used as the excitation of the complete PEU assembly. The system is fixed at its housing attachment points, and the profile of 1N from the lower edge of the frequency range, referred to as f_1, to the upper edge, referred to as f_2, is applied at those locations (as reported above, the entire inverter is not represented: on the housing, there are attachment points with which the inverter is fixed to other components, and in the simulations conducted, such points have been fixed and the force profile has been here applied). For the frame, a tetrahedral mesh made of TET10 elements is used, while for the PCB, a hexahedral mesh made of HEX20 elements is employed. Structural damping of 1% is applied to the entire inverter structure, while no structural damping is included in the TVAs. The forced response is computed via mode-based steady state simulation in Ansys.

It is worthwhile to note that the stop band generated by the resonators can be increased by the addition of damping, however the maximum attenuation achieved in this case is lower than the maximum attenuation obtained when damping is absent in line with findings in literature [6], [19]. In section 6, instead, where the real resonators have been applied to the structure, 5% structural damping has been included in the resonator's material properties.

Fig. 3 shows the averaged spectral displacement responses recorded on the upper surface of the PCB in the out-of-plane mode direction. The base configuration, i.e., without the presence of TVAs is also shown for reference.

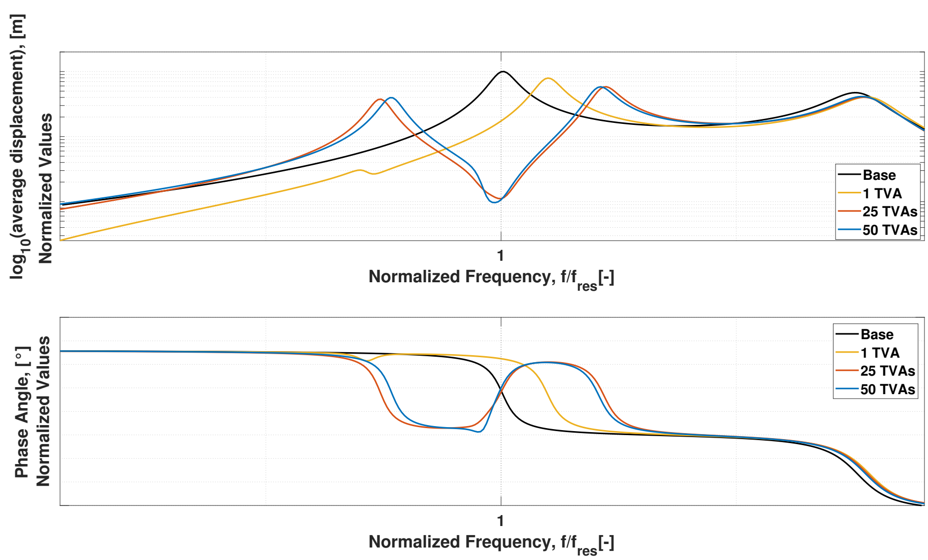

Fig. 3 The average of the directional displacement responses (amplitude and phase in normalized values) recorded on the upper face of the PCB. Frame without TVAs (Base), with 1, 25 and 50 TVAs configuration cases.

The displacement responses represented in amplitude and phase across a range of frequencies reveal different behavior among the configurations, even though the total added mass is consistent. This is expected since locations of each resonator acting on the targeted mode are different.

The single TVA configuration shows a shift in the peak frequency to a slightly higher value with a slight reduction in amplitude, indicative of a basic yet effective vibration mitigation strategy. In contrast, the configurations with 25 and 50 TVAs exhibit a more complex response, characterized by the emergence of dual peaks, one before and the other after the f_{res} frequency. This dual-peak phenomenon, also confirmed by the phase change, suggests an enhanced reduction effect, due to the distributed nature of the TVAs. Additionally, the amplitude of these peaks is reduced as compared to both the base case and the single TVA configuration, highlighting the superior efficiency of the LRM configurations. Interestingly, the similarity in response between the 25 and 50 TVAs configurations suggests a saturation effect, where additional TVAs beyond a certain point do not contribute significantly to further reduction enhancement. Optimal placement and quantity of TVAs can hence be marked as crucial factors in maximizing vibration mitigation. The boundary conditions of the frame, rigidly attached to the external part of the PEU assembly also likely contribute to this effect through emphasis on the predominant role of the central area in the system's vibrational response: due to the fixing of the frame on the PEU housing, it is indeed observed that the central area is more susceptible to deformation, while in the lateral parts, close to the attachment points, such deformation is almost nonexistent. In the configuration with 50 TVAs, therefore, those placed near the attachment points to the housing do not produce an effect comparable to those located in the central part, and it is for this reason that the two configurations exhibit similar behaviors. Furthermore, as previously discussed, the presence of structural damping in the TVAs is expected to reduce the prominence of the first and second peaks in the LRM configuration. This will result in less pronounced attenuation, leading to a broader stop band.

This preliminary study highlights the attenuation introduced by the LRM solution compared to the single TVA case. In the following sections, the Unit Cell modeling approach is explained, and the behavior of practically realizable resonators is studied, when applied to the component.

LRM Solution: Unit Cell Modeling And Comparison

Unit Cell (UC) modeling allows for the study of infinite periodic structures by considering a single part, called the Unit Cell, which represents the smallest non-repetitive part [20]. Starting from the single UC, dispersion curves are calculated, providing information about the presence of stop bands, frequency zones where no free wave propagation is possible [6]. Although this type of modeling is applied to the study of infinite periodic structures, it has been shown to be applicable to finite structures as well [17] and has been extensively used to simulate the behavior of a LRM concept on a real component [11], [13], [15], [16], [21].

In the present application case, considering the presence of a finite system and a particularly complex geometry that causes the presence of ribs and holes, a UC modelling approach is not fully representative. Nevertheless, it is used as a rapid and effective method to compare different types of resonators designs, allowing for the selection of the most suitable resonator type and avoiding computationally expensive simulations.

When applying resonant additions to the component, the conditions for stop band behavior are considered. The resonant cells are added to the component on a scale smaller than the structural wavelength to be influenced [6], the net sum of the forces on the hosting structure contributed by a resonator should be non-zero [10], and they should introduce a localized resonant behavior in the host structure [3], [22]. The UC modeling is based on the application of the Bloch-Floquet theorem, and the application of periodic boundary conditions allows for the simulation of the single UC using the Finite Element method (FEM) [23], [24]: for the inverse approach the wavenumbers are imposed and the problem is solved towards the frequencies, while for the direct approach real frequencies are imposed and the eigenvalue problem is solved to the wave propagation constants [20].

The Bloch's theorem considers the response of a single UC to define the response of a periodic system, which is described by the periodicity of the fundamental UC. This is made possible through the definition of an exponential term that defines both the amplitude and the phase change when a waves passes from one UC to the next [21], [23]. This exponential term utilizes the wave vector $\mathbf{k}$ to define the amplitude and the phase change, particularly considering two propagation directions $\mathbf{d}_{\mathrm{x}}$ and $\mathbf{d}_{\mathrm{y}}$. The propagation vector $\boldsymbol{\mu}= (\mu_{\mathrm{x}}, \mu_{\mathrm{y}})$ defines the complex phase shift for a wave propagating along one of the two directions. Eq. (1) gives the relation between the wave vector, the propagation vector, and the direction of propagation:

$$\mu_{\mathrm{i}}=\mathbf{k}\bullet\mathbf{d}_{\mathrm{i}} \tag{1}$$

Therefore, considering that the forces and displacements on the single UC's boundaries can be scaled in the $\mathbf{d}_{\mathrm{x}}$ and $\mathbf{d}_{\mathrm{y}}$ directions using $\mathrm{e}^{\mu_{\mathrm{x}}}$ and $\mathrm{e}^{\mu_{\mathrm{y}}}$, a matrix $\mathbf{R}$ (function of $\boldsymbol{\mu}$) is used to relate the generalized displacement $\mathbf{q}$ to a reduced set of displacement $\mathbf{q}^{\mathrm{red}}$, eq. (2).

$$\mathbf{R}\mathbf{q}^{\mathrm{red}}=\mathbf{q} \tag{2}$$

The same matrix $\mathbf{R}$ can also be used to rewrite the equation of motion, in a matrix form for a steady-state harmonic responses, in terms of the reduced set, eq. (3):

$$\mathbf{R}'\left(\mathbf{K}+\mathrm{j}\omega\mathbf{C}-\omega^2\mathbf{M}\right)\mathbf{R}\mathbf{q}^{\mathrm{red}}=\mathbf{R}'\mathbf{f} \tag{3}$$

where $\mathbf{R}'$ is the conjugate transpose of $\mathbf{R}$. Assuming that no external forces are applied to the internal nodes of the UC and that $\mathbf{K}^{\mathrm{red}}=\mathbf{R}'\mathbf{K}\mathbf{R}$, $\mathbf{C}^{\mathrm{red}}=\mathbf{R}'\mathbf{C}\mathbf{R}$ and $\mathbf{M}^{\mathrm{red}}=\mathbf{M}'\mathbf{K}\mathbf{M}$, the equation can be rewritten as in eq. (4) [26].

$$\left(\mathbf{K}^{\mathrm{red}}+\mathrm{j}\omega\mathbf{C}^{\mathrm{red}}-\omega^2\mathbf{M}^{\mathrm{red}}\right)\mathbf{q}^{\mathrm{red}}=\mathbf{0} \tag{4}$$

By solving the eigenvalue problem in eq. (4), the dispersion curves can be obtained. The three unknowns of the problem are: ω, μ_{x}, μ_{y}. As stated before, the presence of a direct $\boldsymbol{\mu}(\omega)$ and inverse $\omega(\boldsymbol{\mu})$ approach derives from the different resolution that this equation has, as both ω and μ_{x}, μ_{y} can be complex.

- Inverse approach, $\omega(\boldsymbol{\mu})$: the wave vector constants $(\mu_{\mathrm{x}}, \mu_{\mathrm{y}})$ are imposed, and the problem is solved for ω. Free propagation wave is considered, and this type of approach is typically used for undamped UCs (with a damping matrix $\mathbf{C}$ equal to the zero matrix). The resulting frequencies can be real, imaginary or complex representing freely propagating, evanescent or decaying waves [20].
- Direct approach, $\boldsymbol{\mu}(\omega)$: in this case, real ω values are imposed, and the problem is solved with respect to $(\mu_{\mathrm{x}}, \mu_{\mathrm{y}})$. A time-harmonic wave propagation is considered, and the approach is typically used for damped UCs.

For further information regarding this modeling technique and problem resolution using the Inverse and Direct approaches, the interested reader is referred to [6], [23], [24], [26], [27].

In the current study, the methodology of UC modeling through an inverse approach has been applied, including simulations of three distinct two-dimensional (2D) UCs without incorporating damping effects into the calculations. The UCs under examination are illustrated in Fig. 4, which comprises three variants. Fig. 4 presents on the left a UC conceptualized as a single TVA depicted as a mass-spring system and referred to as the TVA UC. On the central and right part, Fig. 4 displays UCs including practical resonator designs, labeled as the Cantilever Resonator UC and the Ring Resonator UC, respectively. The TVA UC configuration represents an idealized scenario, where the mass-spring system serves as a preliminary model, as detailed in section 3. The proper resonators designs are conceptualized for fabrication via Additive Manufacturing techniques: this technology allows to produce resonators bodies and when mass addition is needed, it can be positioned on top of the resonators. For the study presented, the Cantilever Resonator body has been modeled with polylactic acid-based filament (PLA) and the Ring Resonator with thermoplastic polyurethane (TPU). For the supplementary mass, steel has been considered. The following material constants have been employed, taken from commercial material datasheets, and reported in Table 1. For the subsequent creation of the samples, it is necessary to experimentally characterize the values for the indicated materials and to consider the substantial variations that can occur depending on the type of filament chosen or its orientation.

Table 1 Resonators' material properties.

Material	**Young Modulus, E $[Pa]$**	**Poisson Ratio, v $[-]$**	**Density, ρ $[kg/m^3]$**
PLA	$2865\ MPa$	$0,35$	$1240\ kg/m^3$
TPU	$60\ MPa$	$0,4$	$1080\ kg/m^3$
Steel	$193\ GPa$	$0,3$	$8000\ kg/m^3$

In the three studied cases, the selected unit cell measures $0,075x0,105mm$ (lengths normalized with respect to the frame's longest dimension), allowing for the placement of 25 TVAs or resonators as established in preliminary simulations. This configuration also marks the limit for the number of resonators that can be placed on the frame due to the geometric constraints of the structure. The three types of resonators are designed to exert a force perpendicular to the structure: in fact, the out-of-plane waves aim to be affected by these types of resonators.

For the base of the three UCs, SHELL181 elements have been employed. The Cantilever Resonator and Ring Resonator bodies have been modeled using solid HEX20 elements. For the TVA UC, a MASS21 element has been used to simulate the mass component and a COMBIN14 element has been selected for the spring component. Detailed specifications of the models utilized are presented in Table 2.

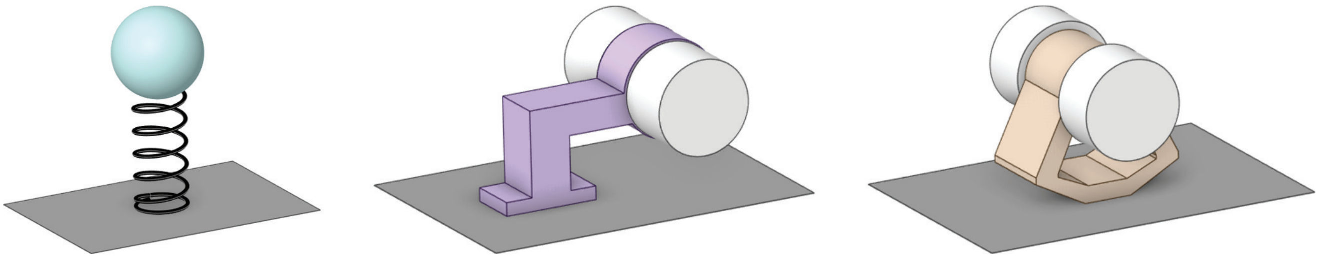

Fig. 4 Unit Cells. Left: TVA UC. Center: Cantilever Resonator UC. Right: Ring Resonator UC.

Table 2 Model specifications. UCs dimensions, mesh element types and mesh element number employed.

Type of UC	UC Length (mm)	Mesh elements (type)	Mesh elements (number)
TVA UC	0,075x0,105	Base: SHELL181 Mass: MASS21; Spring: COMBIN14	Base: 1800 Mass: 1; Spring:1
Cantilever Resonator UC	0,075x0,105	Base: SHELL181 Body: HEX20	Base: 1607 Body: 1572
Ring Resonator UC	0,075x0,105	Base: SHELL181 Body: HEX20	Base: 1628 Body: 1649

In the case of the TVA UC, the mass-spring configuration contributes an additional 15% mass to the base UC and exhibits resonance at the frequency $\mathrm{f_{res}}$. The analysis of dispersion curves, along the Irreducible Brillouin Contour (IBR) delineated as O, A, B, C, O and representing a transition through the points (0,0), (0,π), (π,π), (π,0), (0,0), is shown in Fig. 5. The IBR is defined as the smallest region within the wave domain that contains all essential information: given the periodic nature of the structure under examination, its properties related to dispersion surfaces are also periodic and this periodicity justifies the reduction to the IBR for assessing the presence of stop bands [23]. Dispersion curves for the TVA UC are derived and depicted in Fig. 5. The area marked in light blue represents the stopband for the target frequency range and exhibits a bandwidth that will be addressed as $\mathrm{f_{Band,TVA}}$. This region is defined by two boundaries corresponding to the out-of-plane flexural waves (indicated in orange). The TVA hence creates a stopband centered around $\mathrm{f_{res}}$, which denotes the frequency corresponding to the out-of-plane modal response of the component.

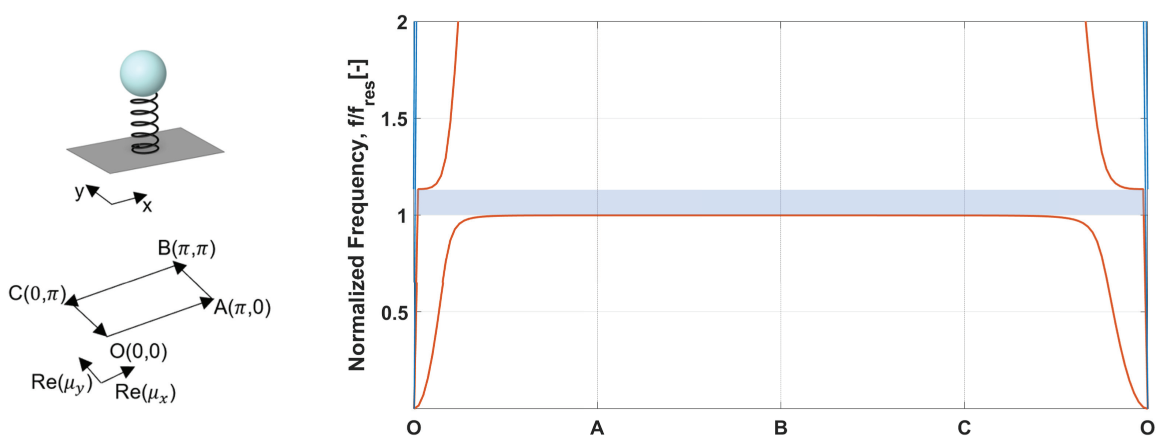

Fig. 5 Top left: Representation of the TVA UC. Bottom left: The IBR used in the computation. Right: Computed dispersion curves.

The fundamental UCs and their dispersion curves for the Cantilever Resonator UC, (Fig. 6), and the Ring Resonator UC, (Fig. 7), have been also analyzed. In these analyses, a mass equivalent to 15% of the UC base is added, and the resulting stop-band widths have been compared to those obtained for the TVA UC. The stop-band width for the Cantilever

Resonator UC is called $f_{Band,Cant}$ and its value is the 77% of $f_{Band,TVA}$, whereas for the Ring Resonator UC, it is named $f_{Band,Ring}$ and its value is the 94% of the $f_{Band,TVA}$. Evidently, latter is notably closer to the stop-band width achieved with an idealized TVA. Although the added mass is consistent across all three cases, the stop-band widths vary, particularly for the Cantilever Resonator. This difference is attributed to the significantly higher Effective Modal Mass (EMM) in the out-of-plane direction for the Ring Resonator compared to the Cantilever Resonator. This higher EMM results in the Ring Resonator approximating the idealized TVA more closely, as is also demonstrated in [28]. Specifically, the EMM in the out-of-plane direction for the Cantilever Resonator is 81% of that of the idealized TVA, while the relative EMM for the Ring Resonator is 97%. Consequently, the stop-band width for the Ring Resonator more closely aligns with that of the idealized TVA. In an idealized TVA, an increase in mass (analogous to the modal effective mass in the out-of-plane direction for real resonators) correlates with an increase in stop-band width, consistent with observations by Claeys et al. [6]. Therefore, the Ring Resonator is selected for further implementation and results on the component under test are discussed in the subsequent section of this study.

Also illustrated in Fig. 6 and Fig. 7 are the fixed base mode shapes of the two resonators. For the Ring Resonator, the mode shape depicted in Fig. 6 corresponds to the first resonance frequency of the system. An examination of the dispersion curves in Fig. 6, shows that the stop band, highlighted in light blue, originates from the first visible waveform on the diagram, which marks the lower limit of the stop band. This stop band is defined by two lines corresponding to the

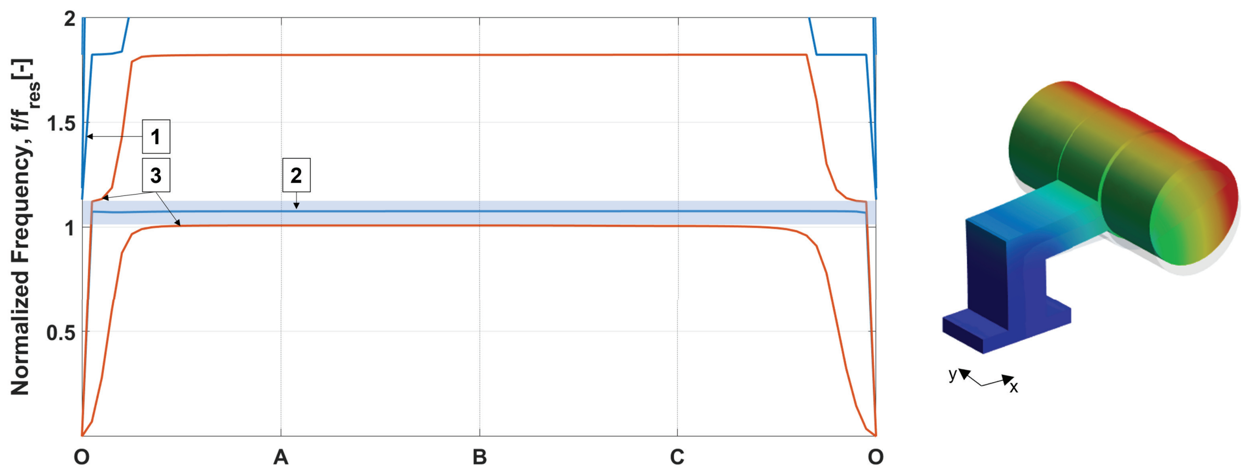

Fig. 6 Left: Cantilever Resonator UC Dispersion Curves. Right: Cantilever Resonator mode shape.

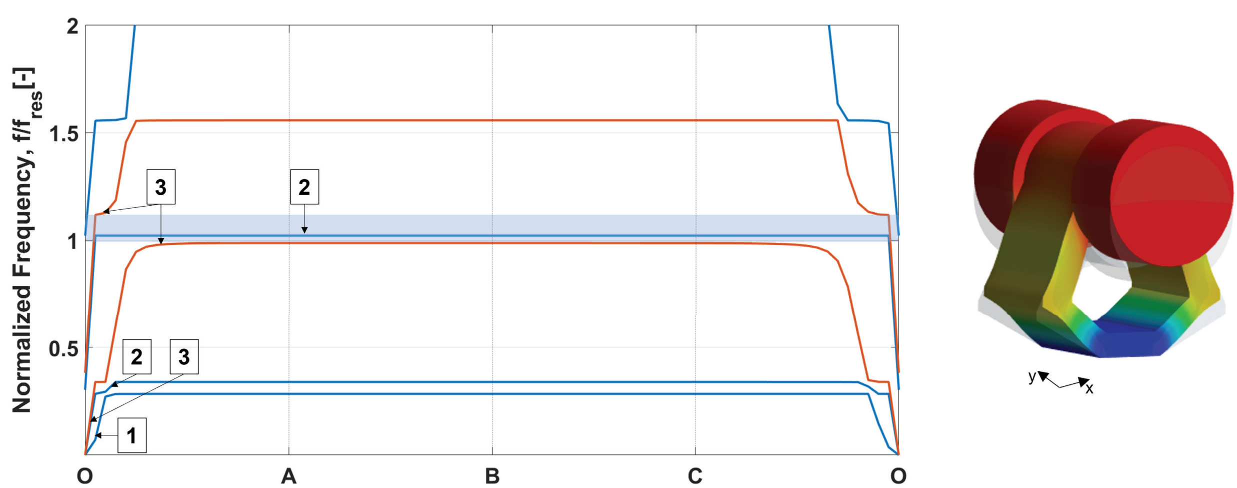

Fig. 7 Left: Ring Resonator UC Dispersion Curves. Right: Ring Resonator mode shape.

out-of-plane flexural waves, labeled in orange as "3". The diagram also includes other types of waveforms (in blue), particularly longitudinal (labeled as "1") and shear ("2"). However, these waveforms develop and impact the system in-plane rather than out-of-plane. To influence the global flexural out-of-plane mode of the component, it is necessary to implement the LRM concept such that the resonators generate a stop band to affect the same. Therefore, out-of-plane flexural waves created by the resonators are especially considered.

With regard to the Ring Resonator in Fig. 7, the obtained dispersion curves show a different shape, featuring a greater number of waveforms within the same frequency range. In this case, examining Fig. 7, "1" corresponds to longitudinal waves, "2" to shear waves, and "3" to bending waves (also in this case the out-of-plane flexural waves are indicated in orange and the other waves types in blue). Here too, the stop band occurs at the resonance frequency (f_{res}) for out-of-plane flexural waves, denoted by "3". At lower frequencies (below $0.5f_{res}$), other curves and bandgaps are visible, which are not observed in the case of the Cantilever Resonator. For the Ring Resonator, the mode shape shown in Fig. 7 corresponds to its third resonance frequency. The first mode shape involves oscillation along the y-axis, and the second along the x-axis (axes are indicated in Fig. 7). The considered mode, tuned to f_{res}, involves a vertical mode along the z-axis, which results in a higher relative EMM compared to the Cantilever Resonator case. Thus, the various curves present below $0.5f_{res}$are in-plane waveforms generated by the first two resonance frequencies of the Ring Resonator and in this case, no flexural wave gaps are obtained. The bandgap of interest for the out-of-plane flexural wave is instead obtained at f_{res}. In this scenario as well, the out-of-plane flexural waves depicted in the diagram are those capable of generating the stop band for the application of interest.

LRM Implementation On The Real Component

In the final section of this study, the implementation of the selected Ring Resonator is detailed. Specifically, 25 resonators, equivalent to the maximum number of Unit Cells (UCs) that can be positioned on the system, have been placed as illustrated in Fig. 8. This study does not present an optimization of the described system, as the focus is to evaluate the potential for vibration reduction using a LRM concept.

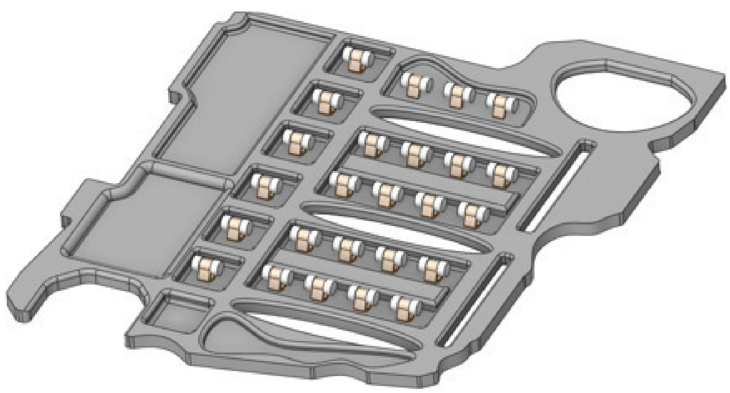

Fig. 8 Frame with LRM Ring Resonators implementation.

Similar to the TVAs discussed in Section 3, the entire system of the PEU has been simulated, and the Ring Resonators have been added to the structure, resulting in a 15% increase in the frame's mass. The system has been secured at the housing attachment points, and a constant acceleration profile of $1 m/s^2$ has been applied at these locations as Base Excitation (to facilitate future experimental replication on a shaker). The results are presented as the average of the displacements on the upper face of the PCB. The Ring Resonators, selected as the optimal solution through UC modeling, are simulated (i) without including structural damping among the material properties of the resonators, and (ii) including a structural damping of 5%. Fig. 9 displays the results for the simulations conducted. As with the case presented in Section 3, the black curve represents the base system, the orange curve depicts the system's response when the 25 Ring Resonators, without the inclusion of 5% structural damping, and the blue curve the response of the LRM solution with the 5% structural damping inclusion.

The outcomes are seen to be comparable and in agreement with the results from the simulation of the 25 TVAs. The amplitude of the peak at the resonant frequency (f_{res}) is reduced, and two distinct peaks are present before and after it, representing in general the in-phase and out of phase modes of the resonators. The presence of this dual-peak phenomenon is confirmed by the phase as well. For the damped resonator case, the reduction achieved is even larger as the two peaks are present but significantly reduced in amplitude compared to the case without structural damping. As for the reduction achieved at f_{res}, the peak attenuation is higher than that of the case without damping. This is in accordance with references [6], [19].

Considering the results of the system's frequency response when TVAs are applied (ideal case, shown in Fig. 3) and the LRM solution (Fig. 9), it is possible to compare the width of the stopband, considered in this case as the frequency range for which the orange curve (in Fig. 3 representing the solution with 25 TVAs and in Fig. 8 the LRM solution without damping) is positioned below the black one (baseline case for both figures). The stopband obtained when the LRM concept is applied to the actual system turns out to be 92% of the solution that involves the 25 TVAs applied to the same system. It should be noted that, in the case of the simulation related only to the UCs and the computation of the dispersion curves, this percentage was around 94%. Therefore, the simulations conducted have demonstrated the feasibility of creating an LRM concept using designs that are practically manufacturable and whose behavior closely approximates the ideal case simulated in Section 3.

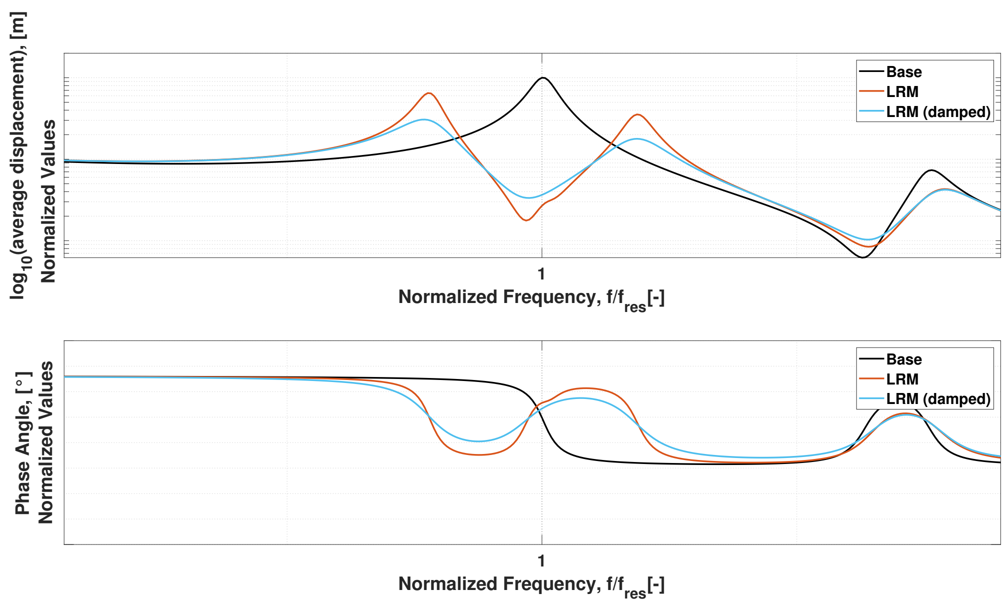

Fig. 9 The average of the directional displacement responses (amplitude and phase in normalized values) recorded on the upper face of the PCB. Frame without LRM concept (Base), LRM concept (LRM) and LRM concept with structural damping (LRM (damped)).

Conclusions

In the presented study, a solution involving LRM applicable to an electric drive PEU is investigated. The problem statement is defined in Section 2, such that an out-of-plane PCB mode, with a global assembly participation is targeted. Key challenges are the physical constraints due to the complex geometry of the component and the requirement to investigate a realizable solution.

The LRM solution is compared to the effectiveness of a single TVA exploring the optimal solution applicable to the component keeping additional mass consistent. This comparison establishes the LRM concept as the superior solution and although the single TVA has an impact on the system, the reduction in component response is less than that achieved with the LRM concept. A comparable reduction is achievable with a single TVA however, this approach is impractical due to the excessive increase in mass on the system at a single location. The proposed optimal resonator is achievable through additive manufacturing technology and capable of being positioned on the frame, while respecting the geometric constraints of the structure.

UC modeling is presented to evaluate initial designs, and different UCs with two types of realizable resonators are simulated and compared, also in relation to an idealized TVA. The Ring Resonator is selected as the optimal solution and its application to the component in a distributed sense is discussed. The results demonstrate its reproducibility in a real case using actual materials and manufacturing technologies.

The numerical study presented indicates that LRMs have potential for application in electronic devices to enhance their reliability and lays the groundwork for a possible experimental study of the considered system. Next steps include experimental characterization of the materials usable for stable production processes of the LRM solutions and experimental validation of the proposed solutions via shaker and vehicle testing for the electric drive PEU.

Acknowledgments The authors gratefully acknowledge the European Commission for its support of the Marie Sklodowska Curie program through the GAP_NOISE project (GA No. 101073014). Views and opinions expressed are however those of the authors only and do not necessarily reflect those of the European Union. The European Union cannot be held responsible for them. Internal Funds KU Leuven are gratefully acknowledged for their support.

References

1. Gharaibeh, M. A. “Reliability analysis of vibrating electronic assemblies using analytical solutions and response surface methodology”. Microelectronics Reliability, Vol. 84, pages 238–247 (2018)
2. Wong, E. H., Seah, S. K. W., Shim, V. P. W. “A review of board level solder joints for mobile applications”. Microelectronics Reliability, Vol. 48, No. 11–12, pages 1747–1758 (2008)
3. Wong, E. H., Lim, K. M., Lee, N., Seah, S., Hoe, C., Wang, J. “Drop impact test - mechanics & physics of failure”. 4th Electronics Packaging Technology Conference, pages 327–333, (2002)
4. Can, F., Gurbuz, Y., Ozaydin Ince, G. “An adhesion promoter layer for high-frequency printed circuit boards (PCBs) via initiated chemical vapor deposition”. Materials Today Communications, Vol. 40, page 109559 (2024)
5. Chen, Y. S., Lai, H. K., Lin, T. C., Chang, P. H., Jen, M. U. “Analyses of printed circuit boards subjected to vibration loadings under various clamping types and reinforced ribs”. 2015 10th International Microsystems, Packaging, Assembly and Circuits Technology Conference (IMPACT), pages 378–381 (2015)
6. Claeys, C. C., Vergote, K., Sas, P., Desmet, W. “On the potential of tuned resonators to obtain low-frequency vibrational stop bands in periodic panels”. Journal of Sound and Vibration, Vol. 332, No. 6, pages 1418–1436 (2013)
7. Liu, L., Hussein, M. I. “Wave Motion in Periodic Flexural Beams and Characterization of the Transition Between Bragg Scattering and Local Resonance”. Journal of Applied Mechanics, Vol. 79, No. 1, pages 011003 (2012)
8. Kittel, C. “Introduction to solid state physics”. (2005)
9. Goffaux, C., Sánchez-Dehesa, J., Yeyati, A. L., Lambin, Ph., Khelif, A., Vasseur, J. O., Djafari-Rouhani, B. “Evidence of Fano-Like Interference Phenomena in Locally Resonant Materials”. Physical Review Letters, Vol. 88, No. 22, pages 225502 (2002)
10. Wang, G., Wen, X., Wen, J., Shao, L., Liu, Y. “Two-Dimensional Locally Resonant Phononic Crystals with Binary Structures”. Physical Review Letters, Vol. 93, No. 15, pages 154302 (2004)
11. Van Belle, L., Sangiuliano, L., Rocha de Melo Filho, N. G., Clasing Villanueva, M., Boukadia, R., Ahsani, S., Alves Pires, F., Zhang, Z., Claeys, C., Deckers, E., Pluymers, B., Desmet, W. “Vibro-Acoustic Metamaterials for Improved Interior NVH Performance in Vehicles”. Future Interior Concepts, pages 31–51 (2021)
12. Wu, X., Sun, L., Zuo, S., Liu, P., Huang, H. “Vibration reduction of car body based on 2D dual-base locally resonant phononic crystal”. Applied Acoustics, Vol. 151, pages 1–9 (2019)
13. Sangiuliano, L., Claeys, C., Deckers, E., De Smet, J., Pluymers, B., Desmet, W. “Reducing Vehicle Interior NVH by Means of Locally Resonant Metamaterial Patches on Rear Shock Towers”. SAE Technical Paper, pages 2019-01–1502 (2019)
14. Sangiuliano, L., Reff, B., Palandri, J., Wolf-Monheim, F., Pluymers, B., Deckers, E., Desmet, W., Claeys, C. “Low frequency tyre noise mitigation in a vehicle using metal 3D printed resonant metamaterials”. Mechanical Systems and Signal Processing, Vol. 179, pages 109335 (2022)
15. Chang, K.-J., Jung, J., Kim, H.-G., Choi, D. R., Wang, S. “An Application of Acoustic Metamaterial for Reducing Noise Transfer through Car Body Panels”. SAE Technical Paper, pages 2018-01–1566 (2018)
16. Riess, S., Droste, M., Manushyna, D., Melzer, S., Druwe, T., Georgi, T., Atzrodt, H. “Vibroacoustic Metamaterials for enhanced acoustic Behavior of Vehicle Doors”. 2021 Fifteenth International Congress on Artificial Materials for Novel Wave Phenomena (Metamaterials), pages 374–376 (2021)
17. Claeys, C., Rocha de Melo Filho, N. G., Van Belle, L., Deckers, E., Desmet, W. “Design and validation of metamaterials for multiple structural stop bands in waveguides”. Extreme Mechanics Letters, Vol. 12, pages 7–22 (2017)
18. Steijvers, K., Claeys, C., Van Belle, L., Deckers, E. “Improving Locally Resonant Metamaterial Performance Predictions by Incorporating Injection Moulding Manufacturing Process Simulations”. Recent Trends in Wave Mechanics and Vibrations, Vol. 125, pages 672–680 (2023)
19. Van Belle, L., Claeys, C., Deckers, E., Desmet, W. “On the impact of damping on the dispersion curves of a locally resonant metamaterial: Modelling and experimental validation”. Journal of Sound and Vibration, Vol. 409, pages 1–23 (2017)
20. Cool, V., Deckers, E., Van Belle, L., Claeys, C. “A guide to numerical dispersion curve calculations: Explanation, interpretation and basic Matlab code”. Mechanical Systems and Signal Processing, Vol. 215, pages 111393 (2024)
21. Sangiuliano, L., Claeys, C., Deckers, E., Pluymers, B., Desmet, W. “Force Isolation by Locally Resonant Metamaterials to Reduce NVH”. SAE Technical Paper, pages 2018-01–1544 (2018)
22. Claeys, C., Deckers, E., Pluymers, B., Desmet, W. “A lightweight vibro-acoustic metamaterial demonstrator: Numerical and experimental investigation”. Mechanical Systems and Signal Processing, Vol. 70–71, pages 853–880 (2016)
23. Brillouin, L. “Wave propagation in periodic structures: electric filters and crystal lattices”. (1946)
24. Mead, D. M. “Wave propagation in continuous periodic structures: research contributions from southampton, 1964–1995”. Journal of Sound and Vibration, Vol. 190, No. 3, pages 495–524 (1996)

25. Bloch, F. “Über die Quantenmechanik der Elektronen in Kristallgittern”. Zeitschrift fur Physik, Vol. 52, No. 7–8, pages 555–600 (1929)
26. Mace, B. R., Manconi, E. “Modelling wave propagation in two-dimensional structures using finite element analysis”. Journal of Sound and Vibration, Vol. 318, No. 4–5, pages 884–902 (2008)
27. Mace, B. R., Duhamel, D., Brennan, M. J., Hinke, L. “Finite element prediction of wave motion in structural waveguides”. The Journal of the Acoustical Society of America, Vol. 117, No. 5, pages 2835–2843 (2005)
28. Alves Pires, F., Wandel, M., Thomas, C., Deckers, E., Desmet, W., Claeys, C. “Improving the Sound Transmission Loss of an Aircraft Ceiling Panel by Locally Resonant Metamaterials”. SAE Technical Paper, pages 2022-01–0960 (2022)